Understanding organic solvent permeation during nanofiltration via electrical impedance spectroscopy (EIS)

(article starts on next page)

Understanding organic solvent permeation during nanofiltration via electrical impedance spectroscopy (EIS)

Angie Qi Qi Ng [a,b], Henry J. Tanudjaja [a,c], Ming Ming Yeo [a], Jia Wei Chew [a,b,d,*]

[a] School of Chemical and Biomedical Engineering, Nanyang Technological University, Singapore 637459, Singapore

[b] Singapore Membrane Technology Centre, Nanyang Environment and Water Research Institute, Nanyang Technological University, Singapore 637141, Singapore

[c] Environmental Science and Engineering, Division of Biological and Environmental Science and Engineering (BESE), King Abdullah University of Science and Technology (KAUST), Thuwal, 23955-6900, Saudi Arabia

[d] Chemical Engineering, Chalmers University of Technology, 412 96, Gothenburg, Sweden

ARTICLE INFO

ABSTRACT

To better understand organic solvent nanofiltration mechanisms, Electrical Impedance Spectroscopy was used to analyze real-time changes in the membrane, which functions as a variable dielectric and exhibits changes in capacitance as the solvent permeates. The 350 kDa membranes were composed of polydimethylsiloxane active layers atop polyacrylonitrile supports, while the two solvents were ethanol and isopropyl alcohol (IPA). Four key differences between the solvents are revealed. Firstly, the flux decline was greater for ethanol because the higher polarity promoted adsorption. Secondly, during filtration, the conductance decreased for ethanol but increased for IPA. Thirdly, increasing pressure increased the membrane thickness for ethanol but not for IPA. Fourthly, the permeation mechanisms vary between the two solvents at different pressures. At the lower initial flux, flux decrease was due to extensive adsorption for ethanol, but to the accumulation of IPA impeding permeation for IPA. For the higher initial flux, the gentler flux decline for ethanol was due to greater membrane swelling, whereas the steeper decline for IPA was due to the high driving force promoting permeation through the DP layer to the membrane substrate. The results here underscore the importance of membrane-solvent interactions in affecting OSN performance.

Introduction

Organic solvents are indispensable as customized media for reaction, isolation, purification, etc. in various industries, case in point being solvent accounting for between 80 and 90 % of mass utilization in the biopharmaceutical industry [1]. The vast employment of organic solvents comes at a price, a significant component of which involves the separation or purification at the intermediate steps and the treatment of the resulting waste streams. Especially for the stringent pharmaceutical industry standards, the high-value intermediates and products must be completely stripped of organic solvents used during synthesis [2]. Despite considerable advances in separation technologies, separations involving organic solvent represents around 60 % of the overall energy consumption in the manufacture of active pharmaceutical ingredients (API) [3]. Notably, it is well-acknowledged that pharmaceutical processes have the highest E-factor [4] (i.e., waste generated per unit product), which represents the first green chemistry metric across the

chemical industry spectrum. This is mainly due to the intricate multi-step synthesis involving high volumes of solvents used to synthesize, isolate, and purify intermediates and APIs, as well as cleaning and conditioning of reactors. As there is a need to enhance solvent recovery techniques to improve energy and cost efficiencies, organic solvent nanofiltration (OSN) or solvent-resistant nanofiltration has emerged as a promising energy-efficient alternative to existing processes [5]. This active search on separation performance of OSN membranes aims to enable new processes and new products.

To date, technology breakthroughs in OSN have offered many advantages over existing methods [6]. However, many challenges persist in the implementation, including organic solvent resistance of the membrane [7] and the lack of predictability of the nanofiltration membrane performance [8]. Also, there is a lack of comprehensive understanding in OSN since past membrane-separation studies have predominantly focused on aqueous environments [9–11]. While the performance of both the porous nanofiltration membranes and dense

nanofiltration membranes can be predicted accurately using respectively the pore-flow and solution-diffusion models in aqueous environments, Bhanushali et al., [12] found mis-matches between predictions and experimental data in organic solvents due to the different interactions between the membrane and specific organic solvents. On top of solvent interactions with the OSN membranes, attention has been directed to the solvent stability of membranes with time. Razali et al., tested the solvent stability of the membranes over 24 h in a cross-flow system [9]. Low et al., also conducted similar tests to investigate the stability, solubility, solvent permeance, swelling, as well as performance of the OSN membrane [10]. A few studies reported that flux and pressure applied obey the solution-diffusion model, but found that high swelling of the membrane affects the non-linearity of the data, which is linked to thermodynamic origins [13,14]. Lavania et al., reported a nonlinear flux-pressure relationship of several non-polar solvents using a polydimethylsiloxane (PDMS) membrane [15]. They inferred that the permeation of solvent through the membrane is influenced by the swelling of the active layer and compaction induced by the pressure. For a water–ethanol mixture, Dencheva-Zarkova et al., found that ethanol retention and permeate flux both increased with operating pressure [16]. Shukla and Cheryan concluded that some membranes lose the rejection capacity at higher pressures but have high rejections at low pressures [17]. To date, the permeation mechanism of the organic solvent is not well understood, specifically with respect to whether solute deposition or membrane compaction or membrane aging is the main contributing factor to the decline in performance of the OSN membrane [11]. This motivated the current study, which focused on experimental investigation of the effect of pure organic solvents on membrane performance in the absence of solute.

Non-invasive techniques have been used to visualize and monitor the structural changes as well as particle deposition onto the membrane surface during filtration, such as ultrasonic time-domain reflectometry (UTDR) [18], optical coherence tomography (OCT) [19–21], direct observation through membrane (DOTM) [22,23] and electrical impedance spectroscopy (EIS) [24,25]. Each has its own advantages and disadvantages [26,27]. For UTDR, OCT and DOTM, they can only be used for monitoring deposition of colloids and particulates but fall short for evaluating solvent permeation. To this end, past studies have demonstrated the capability of EIS to detect real-time changes in membrane structure due to solvent permeation via the changes in conductance or impedance at the different interfaces, which are represented by different ranges of frequencies [28,29]. Specifically, the EIS setup is such that the membrane acts like the electrodes, such that the corresponding impedance models reflects membrane surface characteristics (e.g., porosity), electrical properties of the solutions and the interfacial regions [25]. Correspondingly, EIS has been harnessed to assess various facets of membrane filtration, including investigate the interfacial capacitance and diffusion boundary layer thickness of ion-exchange membranes [28], monitor protein fouling [30], understand the effect of the concentration and type of electrolytes on the active layer [31], and quantify real-time changes of performance parameters of membranes [21].

Exploiting the advantage of EIS, this study represents the first study on using EIS to study pure organic solvent permeation behaviors during cross-flow filtration. Specifically, this study focused on utilizing EIS to understand the permeation of two different organic solvents commonly used in the pharmaceutical industry (namely, *iso*-propyl alcohol (IPA) and ethanol, which are of different polarities) during cross-flow nanofiltration. The pressures implemented in the range of 0.12 – 0.44 MPa are lower than that typical for OSN, but necessarily so to avoid hydraulic compaction effects, and thus focus on how different solvent interactions influence the membrane properties and behavior. The Nyquist plots were analyzed along with the conductance plots to understand the mechanisms underlying the different flux declines resulting from filtering the two solvents at three different initial fluxes.

Materials

Membrane

The GMT-oNF2 (Borsig Membrane Technology GmbH (Germany)) membrane, with a molecular weight cut-off (MWCO) of 350 kDa, was used in this study, because of the reported stability in aromatic, aliphatic hydrocarbons, alcohols, ethers, and ketone systems [32]. The membrane is a silicone polymer-based composite with a polydimethylsiloxane (PDMS) active layer on polyacrylonitrile (PAN) support [33]. The FTIR spectrum of the PDMS active layer is presented in Figure A1. PDMS consists of repeating units of dimethylsiloxane monomers and the polymer chains are randomly oriented, as shown in Fig. 3. The details of the membrane are listed in Table 1.

Chemicals

In this study, ethanol and isopropanol (IPA), which are organic solvents commonly used in the biopharmaceutical industry, were investigated [34]. Both were purchased from Merck Sigma-Aldrich, UK. The physical solvent properties are listed in Table 2.

Experimental method

Principles of EIS

EIS has been used for detection of both membrane compaction and membrane fouling in aqueous environments [30,36]. EIS measures the impedance response across a range of frequencies upon introducing electrical signals. As electrical impedance is one of the ways to evaluate membrane-solvent interaction, EIS can provide insights into the electrical behavior of the membrane in the presence of different solvents. Hence, this provides insights into understanding the influence of pure solvent behavior on the membrane during filtration. The operating principle of the EIS unit has been detailed in previous studies [25,37]. Briefly, the EIS measures the impedance (Z) by injecting a small sinusoidal alternating current i at a series of known amplitude i_0 and frequencies ω into the system:

$$i = i_0 sin(\omega t) \tag{2}$$

$$v = v_0 sin(\omega t - \theta) \tag{3}$$

where v and v_0 are respectively the voltage across the sample and supplied voltage amplitude. The spectrometer uses the phase difference θ between i_0 and v_0 to determine v. The resulting impedance, which contains both real and imaginary parts, can be derived as follows:

$$|Z| = \frac{v_0}{i_0}e^{-j\theta} = \frac{v_0}{i_0}(\cos\theta - jsin\theta) \tag{4}$$

This gives the impedance in terms of the measurable parameters, such as i_0, v_0, θ and the imaginary unit vector, j, where $j^2 = -1$. Since the impedance is complex with both real and imaginary parts, a Nyquist plot can be used to represent the impedance value. Additionally, the values of the real and imaginary parts are inversely proportional to the conductance (G) and capacitance (C) elements [30], which can be calculated as follows:

$$G = \frac{1}{|Z|}\cos\theta \tag{5}$$

$$C = \frac{1}{\omega|Z|}sin\theta \tag{6}$$

Changes in the conductance and capacitance with frequency represent the phenomena happening at the various layers and interfaces of the heterogeneous membrane (namely, diffusion polarization (DP) layer,

Table 1
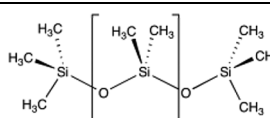Manufacturer specifications of GMT-oNF2 membrane.

Membrane type	Active layer	Support layer	Type	MWCO	Structure
oNF-2	PDMS	PAN	Silicone Composite	350	

Table 2
Physical and solvent properties.

Solvent	Chemical Formula	Polarity index	Molecular weight (g/mol)	Solubility parameter	Specific density (g/ml)	Viscosity (cP)
Ethanol	C_2H_5OH	5.1	46.1	26.2	0.789	1.0
IPA	C_3H_8O	4.3	60.1	23.8	0.783	2.4

the skin layer, the substrate layer and bulk permeate layer) during filtration. Specifically, high frequencies (>100 kHz) represent the bulk solution layer, while the skin layer and substrate layer are represented by frequencies of 10–1000 Hz and 1000–100,000 Hz respectively [38,39]. As for the diffusion polarization layer, it is represented by low frequencies of < 10 Hz [38]. The series of frequency ranges is analogous to the electrical representation in the Maxwell-Wagner model [24]. The Maxwell-Wagner element is as shown:
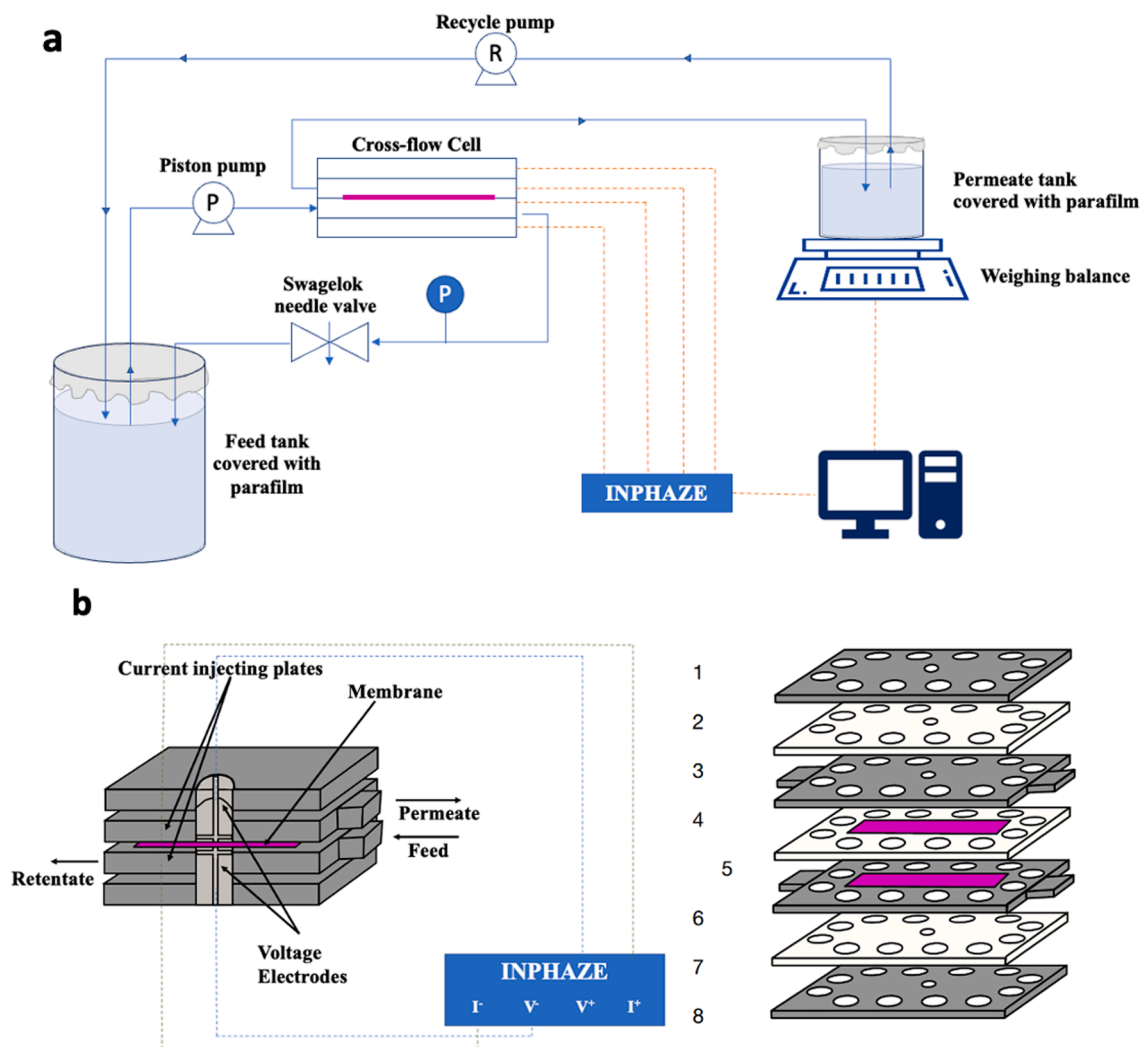

Fig. 1. (a) Crossflow NF filtration setup with real-time EIS monitoring; and (b) cross-section of the crossflow NF-EIS membrane cell linked to the INPHAZE[TM] spectrometer. 1,3,6 and 8 are stainless steel plates; 2, 4 and 7 are insulating plastic plates and 5 is the membrane. 4 has the hole in the middle which is in the shape of the membrane to provide the structural support to hold the membrane in place during the filtration experiment. 4 helps to establish a fix distance between the membrane and the electrodes such that the active surface area of the membrane is always in contact with the fixed amount of solvent and metals plates 3 and 6.

$$Z(\omega) = \frac{1}{G + j\omega C} \tag{7}$$

After fitting the recorded impedance data according to the Maxwell-Wagner model, $Z(\omega)$ can be re-cast as follows to derive the C and G values of each layer:

$$Z(\omega) = \frac{G}{G^2 + C^2\omega^2} - J\frac{C_\omega}{G^2 + C^2\omega^2} \tag{8}$$

The complex variable, Z, consists of a real part (Z_{Re}) and an imaginary part (Z_{lm}), where $= Z_{Re} - jZ_{lm}$. Thus,

$$Z_{Re} = \frac{G}{G^2 + C^2\omega^2} \text{ and } Z_{lm} = \frac{C_\omega}{G^2 + C^2\omega^2} \tag{9}$$

The values of Z_{lm} and Z_{Re} are inversely proportional to the values of C and G, respectively. All these variables reflect the real-time changes in the membrane structure during filtration.

In summary, EIS provides valuable insights into the solvent distribution state within the membrane, specifically in the diffusion polarization layer and the membrane substrate layer, through using (i) conductance values to interpret the sorption of solvent molecules onto the membrane surface; (ii) shifts in Nyquist plots to evaluate the mobility of solvent molecules within the membrane; and (iii) changes in impedance to understand the change in hydrophilicity or hydrophobicity of the membrane as well as membrane swelling during solvent permeation. The membrane filtration cell was scanned until the permeate volume reached 30 ml and EIS data were obtained throughout the filtration. Subsequently, these Nyquist plots were analyzed by analogy to the Maxwell-Wagner model to obtain the model parameters using Mathematica to reflect the real-time changes in the membrane structure during filtration.

Crossflow nanofiltration (NF) setup

The crossflow NF setup with real-time EIS monitoring is illustrated in Fig. 1a, with details of the membrane module depicted in Fig. 1b. The feed tank was covered with Parafilm to minimize solvent evaporation throughout the run. The feed was piston-pumped (Eldex Optos, High Pressure Liquid Metering Pump 3HM Model) to the membrane module at a flow rate of 80 ml/min throughout all experiments. The needle valve (Swagelok) was regulated to control the pressure to implement different initial permeate fluxes for the experiments. The transmembrane pressure (TMP) was quantified with a digital pressure gauge (Daiichi Keiki Seisakusho, Model DPM-AS-1 M−0−R2−3) installed in the retentate line. The permeate flux (J) was calculated by recording the mass of the permeate collected every 30 s in a beaker sitting on the weighing balance (Mettler-Toledo; ME4002E):

$$J = \frac{m_t - m_0}{A \times t} \tag{1}$$

where m_t is the permeate mass at time t, m_0 is the permeate mass at $t = 0$, A is the active filtration area of the membrane and t is the time interval between mass data (namely, 30 s). The collected permeate was recycled back to the feed side using a peristaltic pump (Cole Parmer, Masterflex L/S Model) at an interval of 15 ml accumulated volume to maintain the solvent height level in the feed tank. Three different initial permeate fluxes, namely, 2.6 LMH, 5.3 LMH, 8.0 LMH, were set for each solvent by imposing TMP values of 0.12 MPa, 0.25 MPa and 0.44 MPa, respectively. Each initial flux was repeated at least three times to check for reproducibility. Each constant-TMP filtration run was terminated when 30 ml of permeate is collected in the permeate tank.

The membrane module (Fig. 1b) was such that the feed chamber was 150 mm length-wise by 30 mm width-wise by 0.95 mm height-wise, and the effective membrane-filtration area was 0.0045 m². Four electrodes were used for the EIS measurement, with two electrodes to inject and

measure potential and the other pair for current. The measurement was done with a signal reference circuit amplitude and range of 30 mV ± 5 mV and − 10 Ω to 10 Ω, respectively. The electrodes were connected to the INPHAZE™ spectrometer (Sydney, Australia) via NI USB-6356/6366 for impedance measurement and the difference of potential of the membrane system. After the solvent of interest was introduced, a sinusoidal alternating current (AC) between 0.1 Hz and 100 kHz was injected to the membrane cell and the potential developed in the membrane system was measured. The feasibility of impedance and conductivity measurements during crossflow filtration relies on the continuous liquid phase within the membrane; as such, solvent permeation is analogous to electrical transmission. The GMT-oNF2 membrane was placed between plates 3 and 6 (Fig. 1b) to ensure that the detected signals only concerned with the membrane, feed and permeate. Insulator plates 2 and 7 prevent any current leakage between the different components of the EIS setup, while insulator plate 4 has a hole in the middle that is in the shape of the membrane to secure the sides of the membrane during the experiment. The setup was designed to maintain a fixed distance between the membrane and the electrodes, as well as ensure that the active surface area of the membrane was always in contact with a fixed amount of solvent and in contact with metal plates 3 and 6. At a device-specified voltage of 30 mV, the high-resolution EIS Spectrometer used has a phase resolution of 0.001° and an impedance precision of 0.001 %. Each EIS scan took 15 min. EIS Impedance Analyser software (Wolfram Mathematica 12.0 software) was used to do the EIS model-fitting, which was done by calculating the real and imaginary values of the impedance (Z) to create the Nyquist plot as well as the conductance (G) values.

Experimental protocol

The standard experimental protocol for organic solvent nanofiltration [40] was used. First, the GMT-oNF2 membrane was wetted with the pure solvent tested, i.e., either ethanol or isopropanol, by immersing the membrane in the solvent. Subsequently, the OSN membrane was positioned between the metal plates in the filtration cell as illustrated in Fig. 1. The filtration cell was securely sealed to prevent any leakage or bypass of the solvent. Then, the membrane was preconditioned by filtration of the pure solvent for approximately 10 min, which was to eliminate any air bubble or dry spot on the membrane surface. The resulting permeate collected during this initial period was discarded. Finally, the EIS monitoring was initiated to commence data collection. Three repeated tests were carried out at each condition and a fresh membrane was used for each test.

Membrane characterization

Field emission scanning electron microscope (SEM) (JE0L JSM 6701F) was used to analyze the cross-sectional structures of both the original membrane and the membrane after filtration with ethanol and IPA. The surface streaming potentials of the membranes were measured using the Anton Paar SurPASS™ instrument. For this characterization, an electrolyte needs to be in contact with the membrane sample, and thus a constant concentration of 5 mM NaCl at a pH of 5.8 was used. The 5 mM NaCl solution played the role of an electrolyte that continuously dissociated into positive and negative charges. The membrane surface was overall negatively charge, thus attracting positive charges and subsequently negative charges to create an equilibrium in the capillary channel of the electrokinetic analyser. As the electrolyte flowed through the capillary channel, the electrochemical double layer got sheared off, creating an imbalance in charges before and after the electrolyte exited the channel, and thus enabling the measurement of streaming potential of the membrane. Pristine GMT-oNF2 membranes as well as the post-filtration membranes were tested.

Results and discussion

Effect of organic solvent

Noting that IPA and ethanol fluxes have been reported to differ [41,42], the pressure gauge was adjusted to give the same initial permeate fluxes to allow for a fairer comparison. Fig. 2 presents the flux decline curves versus permeate volume for ethanol and IPA at the same initial fluxes of 2.6 LMH. Two observations highlight the different behaviors of the two solvents: (i) the permeate flux decreased more for ethanol, which can be attributed to more ethanol molecules being adsorbed onto the membrane as a result of its higher polarity index (Table 2), which in turn caused the initially hydrophobic surface of the membrane to become more polar [12]; and (ii) the error bars, each of which represent the span of data from three tests at each condition, are larger for ethanol.

Machado et al., [41] and Bhanushali et al., [42] reported that ethanol exhibited higher flux than that of IPA for the MPF-50 nanofiltration membrane, a trend which may appear contrary to Fig. 2. It is important to note that both MPF-50 and oNF-2 membranes are cross-linked PDMS layers upon PAN substrate. However, the degree of cross-linking in the PDMS layer can significantly affect overall membrane characteristics, resulting in variations in separation performance. Also, variations in the method used to create the PDMS layer such as spin-coating or solution casting may affect its properties. Furthermore, the PAN support layer may have different characteristics such as pore size and porosity or mechanical properties, which can impact the overall membrane performance.

For the same membrane used here, the difference in relative fluxes between the two solvents can be ascribed to the different membrane properties that lead to different solubility parameters and surface tension. In Table 3, the Hansen solubility parameters (HSP) are presented [35]. Notably, the HSP value of IPA is relatively more similar to that of PDMS, which has been tied to relatively higher flux [43] and thereby provides affirmation of the results in Fig. 2. Moreover, Robinson et al., [44] reported that surface tension affects solvent flux through the OSN membrane. Lopresto et al., found a smaller surface tension of the membrane with IPA compared to ethanol while permeating through the oNF-2 membrane, which indicates higher affinity between IPA and the membrane, which in turn leads to higher flux [35].

Table 4 shows the membrane contact angles as well as streaming potentials for the pristine membrane and membranes after filtering the solvents at initial fluxes of 2.6 LMH. Fig. A2 shows the contact angle images of the pristine membrane as well as after filtration with both pure ethanol and IPA at three initial fluxes of 2.6, 5.3 and 8.0 LMH. Comparing the effect of ethanol versus IPA, the contact angle was lower

(Table A1) and streaming potentials more negative for the former (Table A2), indicating that the more polar ethanol molecules (Table 2) deposited onto the membrane surface, causing the membrane to become relatively less hydrophobic and more charged.

Ethanol, with a higher polarity index [45], resulted in a higher density of ethanol accumulation onto the membrane surface. While the silicone-based membranes (i.e., PDMS), like the oNF2 membrane, are mostly hydrophobic (Fig. 3a), some hydrophilic portions (e.g., bonded oxygens) are present in the membrane [46]. Upon prolonged contact with the hydrophilic solvent (Fig. 3b), the hydrophilic tails of the PDMS polymer chains are turned and oriented towards the surface due to the presence of hydroxyl groups in the solvent [47], causing the initially hydrophobic surface of the membrane to become more polar and attracting more ethanol molecules to be adsorbed onto the membrane (Fig. 3c). According to Roudman et al., this phenomenon can be ascribed to the reorganization of polymer chains at the top layer of the membrane [48]. As such, a locally polar membrane is formed due to the accumulation of small clusters of hydrophilic groups forming on the membrane surface. As the active layer of the membrane becomes relatively more polar, more ethanol molecules get adsorbed onto the membrane, causing a steeper decrease in flux for ethanol relative to IPA. The same mechanism could happen as well for IPA; however, with the lower polarity index and steric hindrance, the interaction of IPA and membrane is expected to be less, and IPA thus stays as free-moving molecules. This shows the adsorption of solvents onto the membrane during filtration, and thus the importance of solvent-membrane interaction in governing flux-decline behaviors.

The differences in the filtration behaviors of the two solvents are further elucidated with the Nyquist plots in Fig. 4, depicting the real part (Z_{real}) and the imaginary part (Z_{img}) of the impedance (Z) generated with the EIS. Via the EIS, solvent permeation is analogous to electrical transmission. While the real number is contributed by the resistor in the EIS, the imaginary number is contributed by the inductor and capacitor. In the context of membrane filtration, (i) the resistor is associated with the pressure drop when the solvent passes through the membrane, which is tied to the membrane structure and properties as well as the permeation mechanism; (ii) the inductor is associated with the different layers, specifically the ions accumulated on the surface of the diffusion polarization layer; and (iii) the capacitor is associated with the accumulation of ions within the membrane. With respect to the imaginary values, the relative difference indicate the variation in the flow of ions through the system over time, which provides information on the influence of the different solvents during filtration. Specifically, Fig. 4 displays the Nyquist plots obtained at four permeate volumes, namely, 0, 10, 20 and 30 ml during the filtration of ethanol and IPA at initial fluxes of 2.6 LMH. Nyquist plots shift rightwards with respect to the 0 ml reference for ethanol, but leftwards for IPA, indicating the progressive increase in impedance for the former case and decrease for the latter. The increase in impedance during ethanol filtration reflects more adsorption of ethanol molecules onto the membrane, which agrees with the contact angle and streaming potential values in Table 4, and also the steeper flux decline for ethanol as compared to IPA, while the increase of conductance is associated with the free movement of the IPA molecules [49]. The impedance measurement provides insights into the influence of solvent behavior on the membrane and reflects the variations in conductance. For IPA, the decreasing impedance indicates that the increasing conductance values. This indicates that IPA, having a lower polarity index (Table 2), tends to move as free moving ions on the surface of the GMT-oNF2 membrane rather than adsorb onto the membrane.

The different flux declines can also be explained by the normalized conductance against permeate volume plots for both ethanol and IPA. Fig. A3 shows the plots for diffusion polarization (G_{DP}/G_{DP-0}) and membrane support (G_{Mem}/G_{Mem-0}) at initial fluxes of 2.6 LMH. While the PDMS was initially non-conductive, the interactions with the solvents conferred conductivity. Comparing the two solvents, Fig. A3a shows that
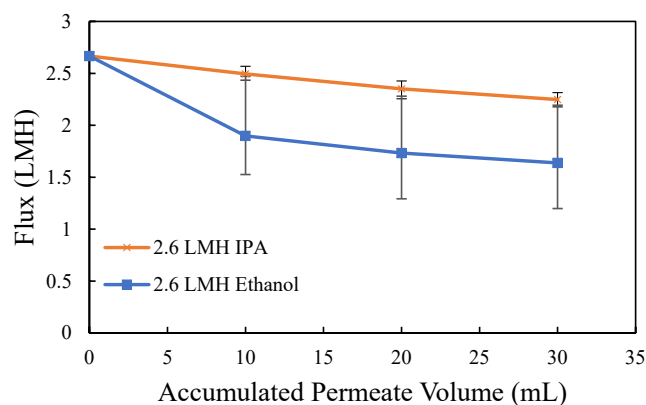

Fig. 2. Flux plotted against accumulated permeate volume for IPA and ethanol. The initial permeate fluxes were consistently 2.6 LMH. The error bars represent the span of data for three tests at each condition.
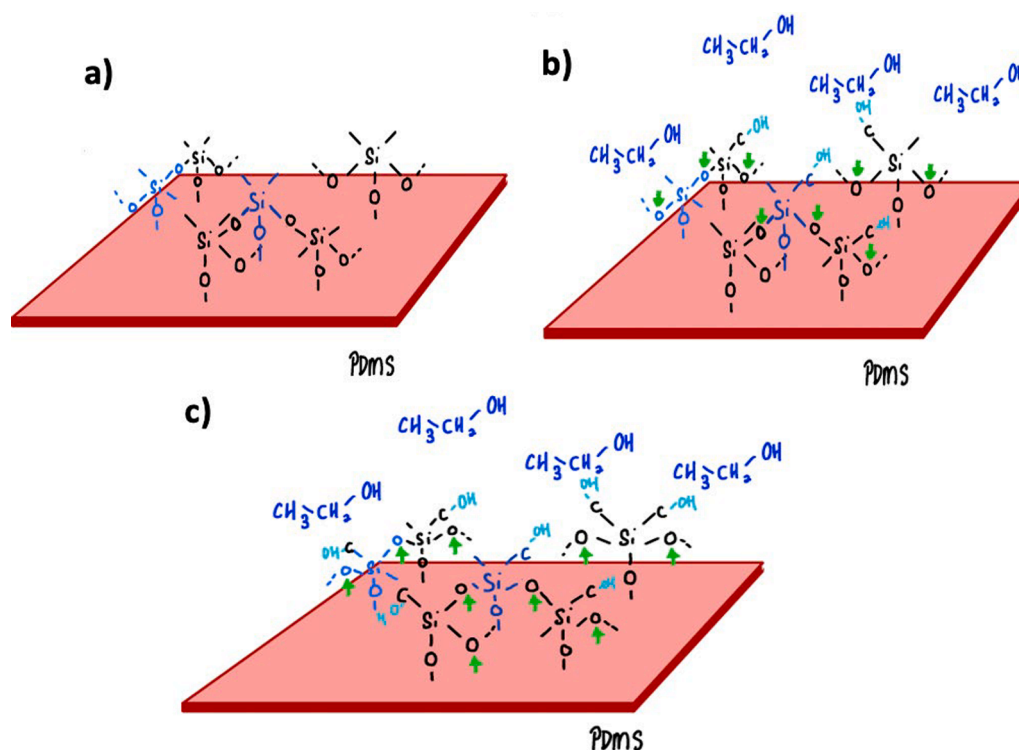
Fig. 3. Schematic on the interaction of ethanol with membrane surface led to the increase of polarity of the membrane surface, which started from normal membrane (a) that interacted with hydrophilic solvent (b), then the hydrophilic part of the membrane turned to the surface and made membrane more polar which attracted more ethanol (c).

Table 3
Hansen solubility parameters (HSP) for solvents and PDMS [35].

Solvent	HSP Parameters			HSP Total
	Dispersion	**Polar**	**Hydrogen Bonding**	
Ethanol	15.8	8.8	19.4	26.52
IPA	16	6.8	17.4	24.60
Polymer				
PDMS	15.9	0	4.1	16.42

Table 4
Membrane contact angles and streaming potentials. The initial permeate fluxes were consistently 2.6 LMH.

	Contact angle (°)	Streaming potentials (mV)
Pristine membrane	108.1 ± 2.0	−31.6 ± 0.2
After filtering ethanol	103.6 ± 1.1	−36.0 ± 1.4
After filtering IPA	106.6 ± 0.1	−30.5 ± 1.0

$G_{DP}/G_{DP\text{-}0}$ rose above 1 for IPA, whereas dropped to around 0.5 for ethanol. This indicates the adsorption of non-conductive ethanol molecules onto the diffusion polarization layer, causing the conductance to drop. On the other hand, the IPA molecules moved as free ions and permeated, rather than become adsorbed onto the surface that contributes to the increase of conductance [49]. Interestingly, at the membrane substrate layer, Fig. A3b shows that $G_{Mem}/G_{Mem\text{-}0}$ significantly rose above 1 for ethanol, reflecting a build-up of ethanol molecules that stayed as free-moving ions in this layer. As for IPA, $G_{Mem}/G_{Mem\text{-}0}$ remained around 1, indicating less build-up of free-moving IPA in the membrane substrate layer and less hindrance of permeation. Although more ethanol molecules were present at the substrate layer, the overall permeation rate was still lower than IPA due to the higher ethanol absorption at the DP or surface layer, which usually becomes the rate-

determining factor for NF membranes [42].

Effect of initial permeate flux

The effect of initial flux during organic solvent filtration on the oNF2 membrane structure was investigated via the Nyquist plots, conductance plots, and difference in thickness values of the active layer between the pristine and post-filtration membranes. Three different operating pressures, which give initial fluxes of 2.6, 5.3 and 8.0 LMH, were imposed for ethanol and IPA permeation. Fig. 5 shows the relationship between initial permeate flux and extent of flux decline. For ethanol (Fig. 5a), the gentlest decline was for the intermediate 5.3 LMH followed by 8.0 LMH, while 2.6 LMH showed the steepest decline. As for IPA, the trend was the other way around, as in the steepest decline was for 5.3 LMH while the gentlest for 2.6 LMH. Notably, the highest initial flux of 8.0 LMH gave intermediate flux decline for both solvents.

Past studies have reported that flux and pressure applied obeys the solution-diffusion model, and that high swelling of the membrane causes non-linearity [13,14]. Fig. 6 presents the data for flux vs pressure for both ethanol and IPA, indicating that the flux-pressure relationships are non-linear for both solvents. In Fig. 6a, the non-linear trend for ethanol agrees with Lavania et al., [15], in which the non-linearity was attributed to membrane swelling. Table 5 affirms the increase of membrane thickness for ethanol and thus membrane swelling. Fig. 6b shows that the less-polar IPA exhibits a relatively more linear flux vs pressure trend. Robinson et al., investigated the permeation of xylene and n-heptane, and similarly found less deviation from linearity [44]. Moreover, Fig. 7 shows the Nyquist plots for the two solvents at initial fluxes of 5.3 and 8.0 LMH. This explains the relationship between the flux decline and the mechanism which takes places on the layers of the membrane upon filtration with the two organic solvents. Furthermore, Fig. 8 displays the normalized conductance versus permeate volume for the diffusion polarization ($G_{DP}/G_{DP\text{-}0}$) and membrane ($G_{Mem}/G_{Mem\text{-}0}$) layers. Fig. A4 shows the conductance versus frequency plots for both solvents at all
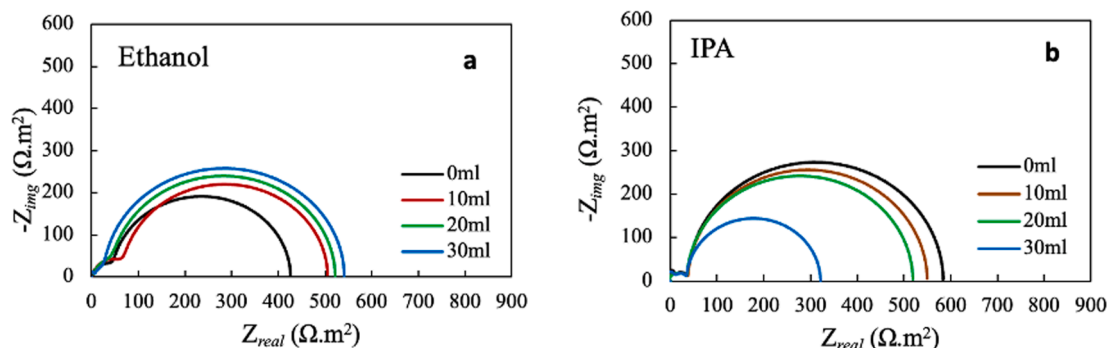
Fig. 4. Nyquist plots for (a) Ethanol, (b) IPA filtered by GMT-oNF2 membranes until 30 ml of permeate was collected. Black lines represent impedance at the start of the experiment. The initial permeate flux was 2.6 LMH in each case.
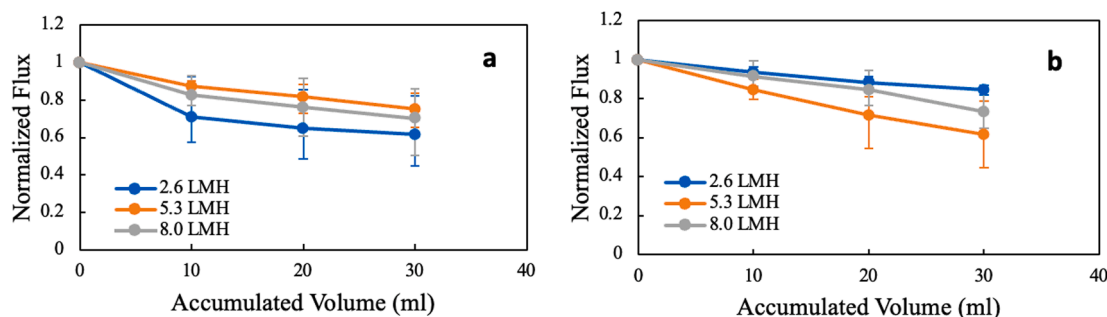

Fig. 5. Normalized flux decline trends at three initial permeate fluxes of 2.6, 5.3, 8.0 LMH for (a) ethanol, and (b) IPA.
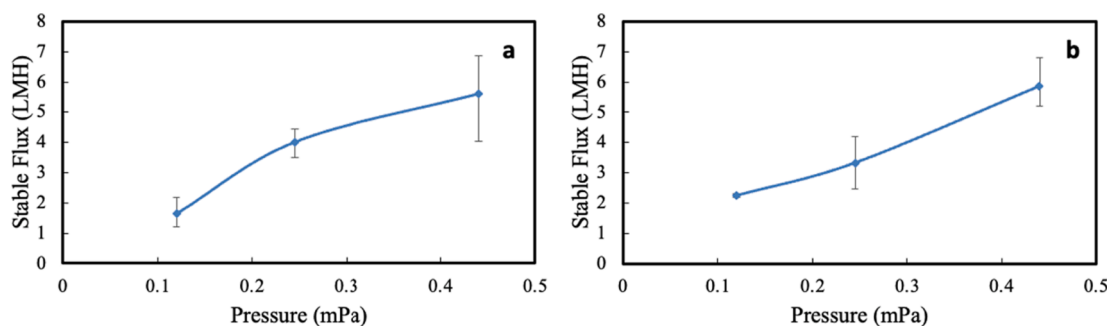

Fig. 6. Stabilized flux vs pressure plots for (a) ethanol, and (b) IPA.

Table 5
Membrane thicknesses after filtration with ethanol and IPA for the three initial permeate fluxes; the pristine membrane thickness was 50.94 $\pm$ 0.62 µm. The values were obtained from FESEM images of the membrane samples (Fig. A5).

Initial Flux (LMH)	Thickness (µm) after filtering ethanol	Thickness (µm) after filtering IPA
2.6	57.98 $\pm$ 0.16	53.91 $\pm$ 0.78
5.3	69.07 $\pm$ 0.63	56.57 $\pm$ 0.05
8.0	73.13 $\pm$ 0.32	57.51 $\pm$ 0.31

three initial fluxes. Fig. 7 shows that the shapes of the Nyquist plots for both solvents at the higher initial fluxes (i.e., 5.3 and 8.0 LMH) are similar. However, as permeation progressed, the plots shift rightwards for ethanol but leftwards for IPA. This suggests that the same mechanisms of absorbed ethanol and free-moving IPA could be present as well at the operating pressures.

Recall that, for ethanol, the gentlest flux decline (Fig. 5a) happened at the intermediate initial flux of 5.3 LMH. Interestingly, Fig. 8a shows that G_{DP}/G_{DP-0} decreased the most for this flux, indicating the most

significant buildup of non-conductive ethanol molecules on the DP layer as filtration progressed. This implies that the least flux decline (Fig. 5a) is tied to the swelling of the membrane that enlarges the membrane pore sizes [50,51]. Somewhat contradictorily, Kappert et al., [52] stated the swelling degree of thin films of PDMS was less in ethanol than IPA (namely, approximately 10 % in ethanol and 30 % in IPA), but that could be due to the prolonged exposure in their study. In this study, membrane thickness increased as the initial flux increased for ethanol, while remained relatively similar for IPA for all initial fluxes 2.6 LMH and above (Table 5). Since the membrane was highly non-polar PDMS, the less-polar IPA was expected to adsorb more extensively onto the membrane to cause more swelling. However, the membrane thickness only increased approximately 3–6 µm for IPA, but increased more to 7–20 µm for ethanol (Table 5). Moreover, Fig. 8c shows that the conductance at the membrane substrate layer (G_{Mem}/G_{Mem-0}) increased with filtration, which suggests that, although more ethanol adsorbed at the DP layer, a higher amount of ethanol molecules still passed through the membrane due to the larger pore sizes of the swelled membrane.

Regarding the highest initial permeate flux of 8.0 LMH (i.e., at the highest pressure imposed), Fig. 8a shows that the decrease in
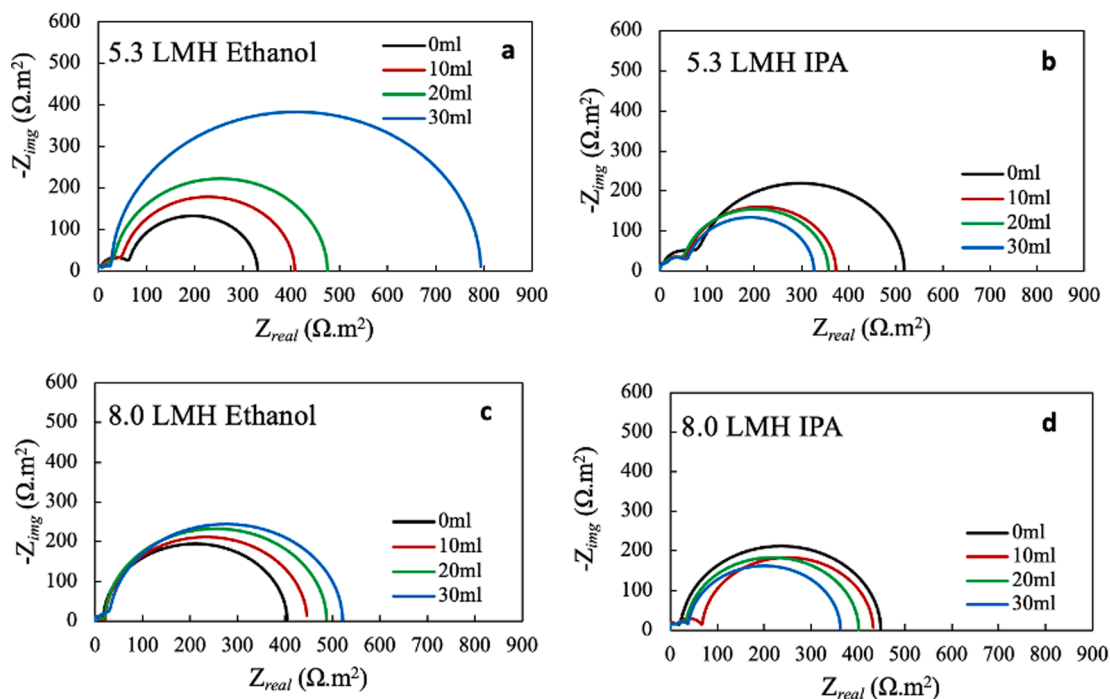
Fig. 7. Nyquist plots for ethanol at initial fluxes of (a) 5.3, (c) 8.0 LMH, and IPA for initial fluxes of (b) 5.3, (d) 8.0 LMH.
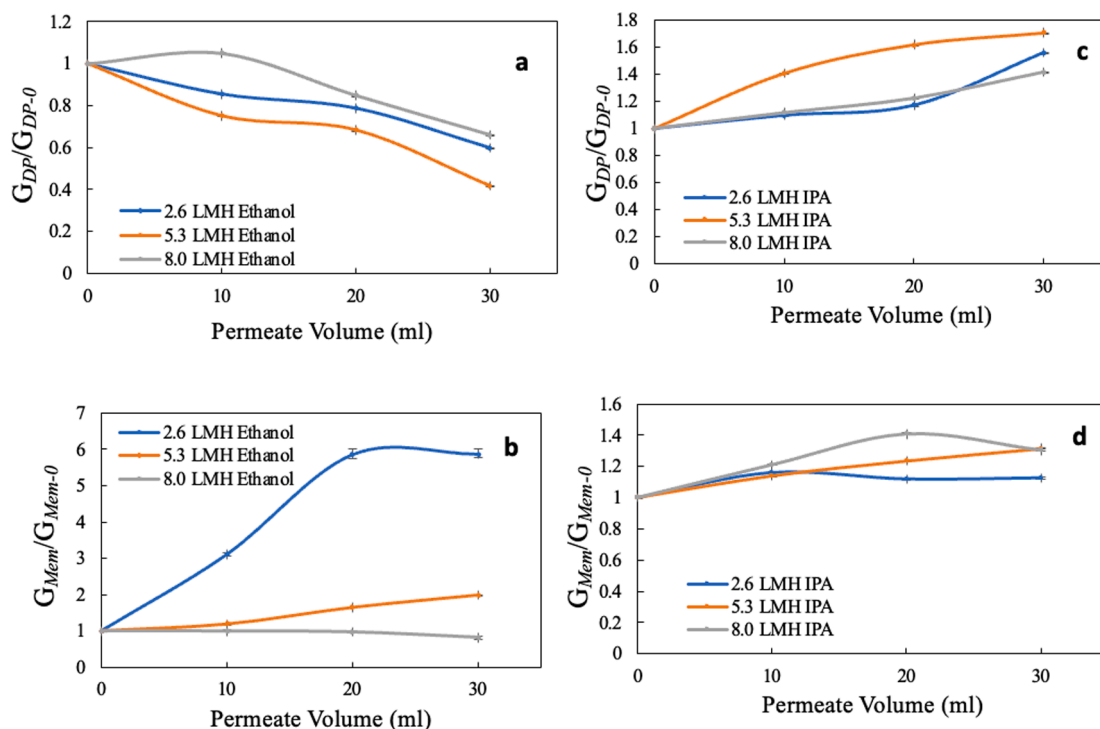

Fig. 8. Normalized conductance versus permeate volume for ethanol for the (a) DP and (b) membrane layers; and for IPA for the (c) DP and (d) membrane layers.

conductance with permeate volume was the least among the initial fluxes, this indicates that the ethanol molecules were least adsorbed onto the membrane surface. Furthermore, Fig. 8b shows that G_{Mem}/G_{Mem-0} decreased, in contrast to the increasing trend for the other two fluxes (i.e., 5.3 LMH and 2.6 LMH). This indicates ethanol molecules accumulated more extensively in the substrate layer at the highest initial flux of 8.0 LMH. The trends in Fig. 8a and b at this initial flux can be tied to the larger pore sizes due to swelling of the membrane structure

[50,51]. The larger pore sizes promote permeation of ethanol relative to adsorption at the membrane surface; however, as the membrane structure swelled, the corresponding increase in thickness caused the permeation rate to decrease. It should be noted that we could not get conclusive pore size distribution results using the liquid displacement porometer, as the pressure required to characterize the pores exceeded the upper pressure limit.

In contrast to ethanol, changes in pressure had negligible impact on

the extent of membrane swelling for IPA, since there was only a change in membrane thickness of approximately 2–6 μm for all initial fluxes evaluated (Table 5). To improve reliability in view of the small measurement area and potential variations caused by sample preparation, FESEM measurements were carried out for different membrane samples from different sets of experiments.

For IPA filtration at the intermediate initial flux of 5.3 LMH, which gave the steepest flux decline (Fig. 5b), Fig. 7b shows that the Nyquist plot shifts significantly even after 10 ml of permeate. This is reflected clearly in Fig. 8c and d, which show that conductance increased for both the DP layer as well as membrane substrate layer from the normalized value of 1. Based on an earlier study that conductance increases as the speed of ion movement increases [49], the increase in conductance here could be due to the faster rate of free-moving IPA ions across the DP layer due to the higher pressure applied to achieve 5.3 LMH. This led to significant accumulation of IPA molecules onto the membrane surface, which impeded permeation and resulted in the steepest flux decline.

As for IPA filtration at 8.0 LMH, the flux decline trend is similar to that at 2.6 LMH. Fig. 8c shows that G_{DP}/G_{DP-0} trends are similar for initial fluxes of 8.0 and 2.6 LMH, implying that there is not much difference in free-moving ions at the DP layer despite the different pressures applied. In contrast, Fig. 8d shows the highest G_M/G_{M-0} at 8.0 LMH, indicating the highest amount of IPA molecules at the membrane layer. Therefore, the EIS results show that, at the highest pressure, more free-moving IPA ions moving at faster rates were in the membrane layer rather than at the DP layer, which suggests that the higher driving force for permeation caused the IPA molecules to penetrate the DP layer, which in turn caused less flux decline than that at 5.3 LMH.

Conclusion

To understand the effect of pure solvent filtration on flux decline and the underlying changes in the different layers of the membrane, EIS was employed during OSN of two common solvents (namely, ethanol and IPA) through GMT-oNF2 membranes in a crossflow filtration setup. The pressures used in the range of 0.12 – 0.44 MPa were lower than typical for OSN to avoid membrane compaction effects and focus on solvent effects. Three different initial fluxes, namely, 2.6, 5.3, and 8.0 LMH, were investigated to assess the effect of filtering different organic solvents. Conductance values allowed interpretation of the sorption of solvent molecules onto the membrane surface, shifts in Nyquist plots allowed for evaluating the mobility of solvent molecules within the membrane, while changes in impedance reflected the change in hydrophilicity or hydrophobicity of the membrane as well as membrane swelling during solvent permeation.

The results show that the more-polar ethanol gave relatively steeper flux declines, which is due to the higher polarity causing the initially hydrophobic membrane to become more hydrophilic. This is not only confirmed by the contact angle and streaming potential values, but also the rightward shifts of the Nyquist plots during ethanol filtration that reflect the decrease in conductance and thus the increase in sorption of ethanol molecules. For the less-polar IPA, the Nyquist plots shift leftwards, indicating an increase in conductance due to free-moving IPA during permeation. This suggests that, even though both are small molecules, the difference in the location of the alcohol group can result into different changes in the layers of the GMT-oNF2 membrane.

This study demonstrates that the changes in the layers of the membrane contributes to different fluxes for the two organic solvents. The more-polar ethanol adsorbed more extensively onto the membrane structure, promoting permeation as the initial flux increased from 2.6 to 5.3 LMH, but then the increase in membrane thickness due to membrane swelling reduced permeation as the initial flux further increased from 5.3 to 8.0 LMH. As for the less-polar IPA that adsorbed less and were more freely moving, the increase in pressure increased the membrane thickness negligibly. The accumulation of IPA on the membrane surface impeded permeation as the initial flux increased from 2.6 to 5.3 LMH, but the increased driving force promoted permeation through the DP layer to the membrane substrate layer as the initial flux increased from 5.3 to 8.0 LMH.

The EIS is shown here to be a valuable tool to reveal that even a slight difference in the chemical structure of the solvent can result in different changes in the layers of the GMT-oNF2 membrane during filtration. This underscores the importance of membrane-solvent interactions on OSN performance. The results are expected to be valuable for understanding the effect of solvent-membrane interactions on OSN performances, and also for improving both OSN membrane fabrication/modification and OSN processes.

CRediT authorship contribution statement

Angie Qi Qi Ng: Methodology, Formal analysis, Investigation, Writing – original draft. **Henry J. Tanudjaja:** Methodology, Formal analysis, Investigation, Writing – original draft. **Ming Ming Yeo:** Investigation. **Jia Wei Chew:** Conceptualization, Methodology, Formal analysis, Investigation, Writing – original draft, Writing – review & editing, Supervision, Project administration, Funding acquisition.

Declaration of competing interest

The authors declare that they have no known competing financial interests or personal relationships that could have appeared to influence the work reported in this paper.

Appendix

Table A1

Contact angles of membranes, with error bars representing the span of two repeat measurements.

Flux (LMH)	Contact angle (°) after filtering ethanol	Contact angle (°) after filtering IPA
0 (pristine)	108.1 ± 0.2	108.1 ± 0.2
2.6	103.6 ± 1.1	106.6 ± 0.1
5.3	100.6 ± 0.1	103.5 ± 0.3
8.0	93.3 ± 0.1	96.1 ± 0.1

Table A2

Streaming potentials of membrane surfaces before and after filtration with ethanol and IPA.

Flux (LMH)	Streaming potential (mV) after filtering ethanol	Streaming potential (mV) after filtering IPA
0 (pristine)	−31.32	−31.32
2.6	−34.75	−32.22
5.3	−32.16	−29.41
8.0	−27.81	−24.11
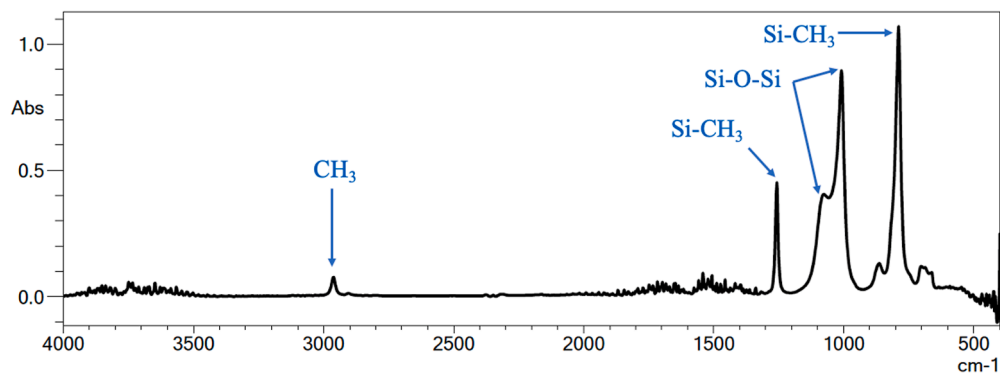
Fig. A1. ATR-FTIR spectra of top layer of GMT-oNF2 membrane
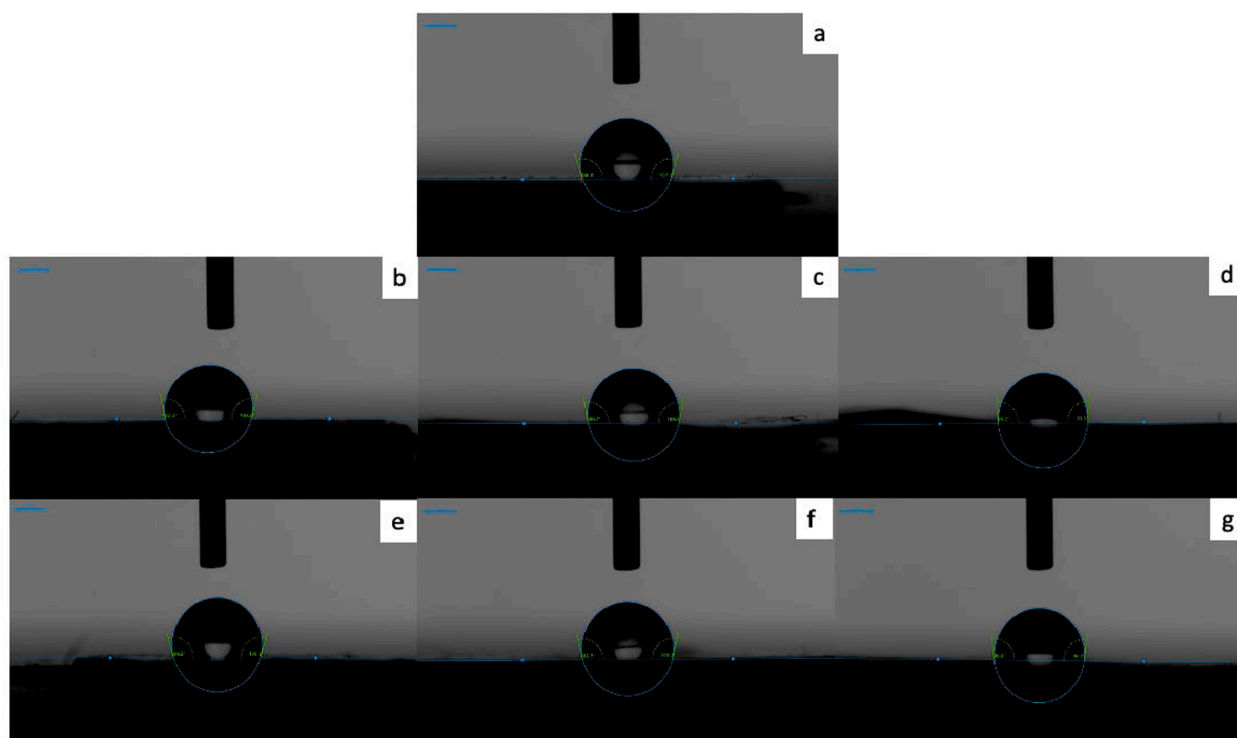
Fig. A2. Images of contact angle of membranes: (a) pristine membrane; membranes after filtering ethanol at initial fluxes of (b) 2.6, (c) 5.3, (d) 8.0 LMH; membranes after filtering IPA at initial fluxes of (e) 2.6, (f) 5.3, (g) 8.0 LMH.
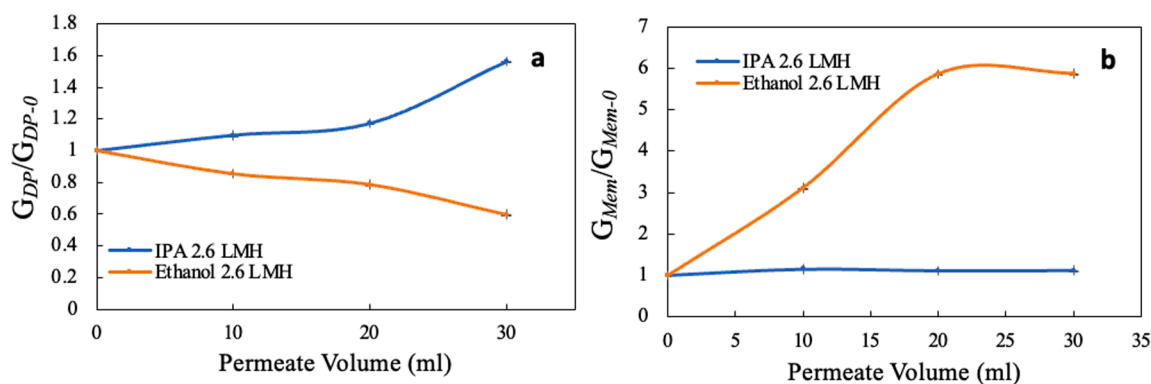
Fig. A3. Normalized conductance versus accumulated permeate volume for IPA and ethanol: (a) DP layer and (b) membrane layer. Constant pressure filtrations were performed at initial fluxes of 2.6 LMH for both IPA and ethanol. The subscript 0 refers to the initial value.
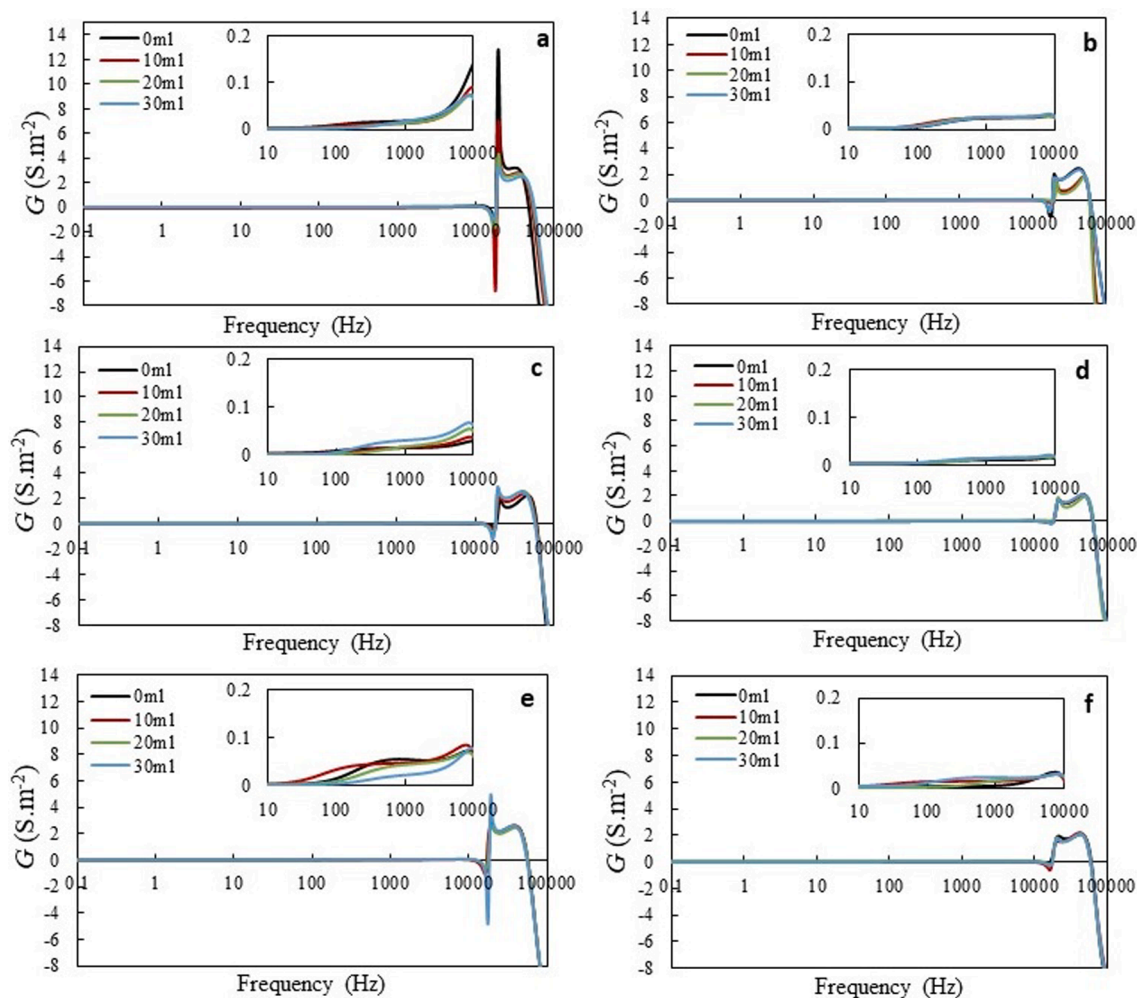

Fig. A4. Conductance versus frequency profiles in the range of 0.1100,000 Hz for ethanol at initial permeate fluxes of (a) 2.6, (c) 5.3, and (e) 8.0 LMH, and IPA at initial fluxes of (b) 2.6, (d) 5.3, and (f) 8.0 LMH. The insets zoom in on the frequency range of 0.1 to 10,000 Hz.
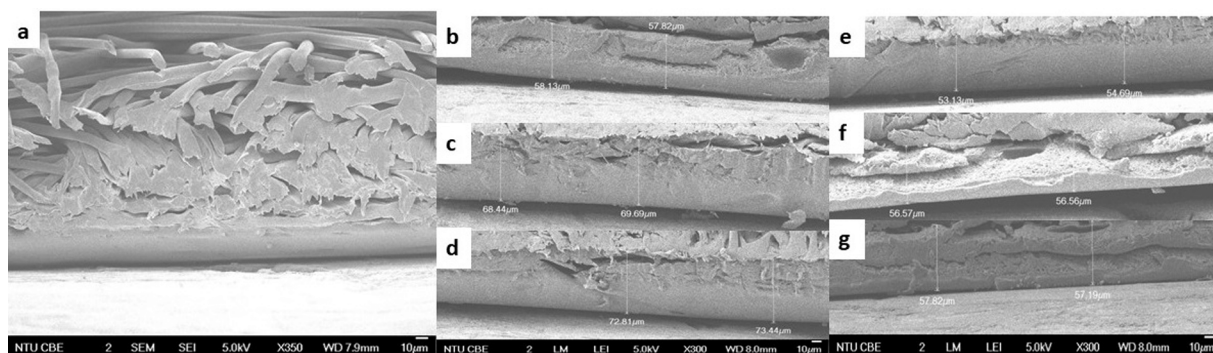
Fig. A5. Cross section of membrane: (a) pristine membrane; after filtering ethanol at an initial permeate flux of (b) 2.6 LMH, (c) 5.8 LMH, (d) 8.0 LMH; after filtering IPA at an initial permeate flux of (e) 2.6 LMH, (f) 5.8 LMH, (g) 8.0 LMH.

References

[1] D.J.C. Constable, C. Jimenez-Gonzalez, R.K. Henderson, Org. Process Res. Dev. 11 (2006) 133–137.
[2] M.G. Buonomenna, J. Bae, Sep. Purif. Rev. 44 (2014) 157–182.
[3] C. Jiménez-González, A.D. Curzons, D.J.C. Constable, V.L. Cunningham, Clean Techn. Environ. Policy 7 (2004) 42–50.
[4] R.A. Sheldon, Chem Commun (camb) (2008) 3352–3365.
[5] M.A. Abdulhamid, G. Szekely, Curr. Opin. Chem. Eng. 36 (2022) 100804.
[6] G. Székely, J. Bandarra, W. Heggie, B. Sellergren, F.C. Ferreira, Sep. Purif. Technol. 86 (2012) 79–87.
[7] P. Silva, S. Han, A.G. Livingston, J. Membr. Sci. 262 (2005) 49–59.
[8] S. Blumenschein, U. Kätzel, Sep. Purif. Technol. 183 (2017) 83–95.
[9] M. Razali, C. Didaskalou, J.F. Kim, M. Babaei, E. Drioli, Y.M. Lee, G. Szekely, ACS Appl Mater Interfaces 9 (2017) 11279–11289.
[10] Z.-X. Low, J. Shen, Sep. Purif. Technol. 256 (2021) 117840.
[11] L.S. White, Curr. Opin. Chem. Eng. 28 (2020) 105–111.
[12] D. Bhanushali, S. Kloos, D. Bhattacharyya, J. Membr. Sci. 208 (2002) 343–359.
[13] D.R. Paul, O.M. Ebra-Lima, J. Appl. Polym. Sci. 15 (1971) 2199–2210.
[14] K.P. Bye, M. Galizia, J. Membr. Sci. 603 (2020) 118020.
[15] J. Lavania, N.K. Rastogi, S. Balaraman, S. Rangaswamy, ACS Omega 6 (2021) 27052–27061.
[16] M. Dencheva-Zarkova, D. Yankov, J. Genova, I. Tsibranska, Bul. Chem. Commun. (2022) 141.
[17] R. Shukla, M. Cheryan, J. Membr. Sci. 198 (2002) 75–85.
[18] R. Sanderson, J. Li, L.J. Koen, L. Lorenzen, J. Membr. Sci. 207 (2002) 105–117.
[19] K.T. Huisman, B. Blankert, H. Horn, M. Wagner, J.S. Vrouwenvelder, S. Bucs, L. Fortunato, J. Membr. Sci. 692 (2024) 122291.
[20] T.A. Trinh, W. Li, Q. Han, X. Liu, A.G. Fane, J.W. Chew, J. Membr. Sci. 548 (2018) 632–640.
[21] L. Gaedt, T.C. Chilcott, M. Chan, T. Nantawisarakul, A.G. Fane, H.G.L. Coster, J. Membr. Sci. 195 (2002) 169–180.
[22] H.J. Tanudjaja, W. Pee, A.G. Fane, J.W. Chew, J. Membr. Sci. 513 (2016) 101–107.
[23] J. Wang, B. Wu, Y. Liu, A.G. Fane, J.W. Chew, J. Membr. Sci. 523 (2017) 409–417.
[24] T.C. Chilcott, A. Antony, G. Leslie, Desalination 403 (2017) 64–79.
[25] T.C. Chilcott, M. Chan, L. Gaedt, T. Nantawisarakul, A.G. Fane, H.G.L. Coster, J. Membr. Sci. 195 (2002) 153–167.
[26] V. Chen, H. Li, A.G. Fane, J. Membr. Sci. 241 (2004) 23–44.
[27] G. Rudolph, T. Virtanen, M. Ferrando, C. Güell, F. Lipnizki, M. Kallioinen, J. Membr. Sci. 588 (2019) 117221.
[28] W. Zhang, J. Ma, P. Wang, Z. Wang, F. Shi, H. Liu, J. Membr. Sci. 502 (2016) 37–47.
[29] J. Li, R.D. Sanderson, Desalination 146 (2002) 169–175.
[30] H.J. Tanudjaja, A.Q.Q. Ng, J.W. Chew, J. Ind. Eng. Chem. 106 (2022) 429–448.
[31] Y. Xu, M. Wang, Z. Ma, C. Gao, Desalination 271 (2011) 29–33.
[32] C.L. Gargalo, I. Udugama, K. Pontius, P.C. Lopez, R.F. Nielsen, A. Hasanzadeh, S. S. Mansouri, C. Bayer, H. Junicke, K.V. Gernaey, J Ind Microbiol Biotechnol 47 (2020) 947–964.
[33] T. Aca Bayrakdar, F. Nahra, D. Ormerod, S.P. Nolan, J. Chem. Technol. Biotechnol. 96 (2021) 3371–3377.
[34] A.P. Katarzyna Grodowska, Acta Polaniae Pharmaceutica - Drug Research 67 (2010) 3–12.
[35] C.G. Lopresto, S. Darvishmanesh, A. Ehsanzadeh, A. Amelio, S. Mazinani, R. Ramazani, V. Calabrò, B. Van der Bruggen, Biofuels Bioproducts and Biorefining 11 (2016) 307–324.
[36] N. Zhang, H.-J. Lee, Y. Wu, M.A. Ganzoury, C.-F. de Lannoy, Sep. Purif. Technol. 288 (2022) 120679.
[37] L.N. Sim, Z.J. Wang, J. Gu, H.G.L. Coster, A.G. Fane, J. Membr. Sci. 443 (2013) 45–53.
[38] J.S. Ho, L.N. Sim, R.D. Webster, B. Viswanath, H.G.L. Coster, A.G. Fane, Desalination 407 (2017) 75–84.
[39] L.N. Sim, J. Gu, H.G.L. Coster, A.G. Fane, Desalination 379 (2016) 126–136.
[40] E. Tsui, J. Membr. Sci. 237 (2004) 61–69.
[41] D.o.R. Machado, D. Hasson, R. Semiat, J. Membr. Sci. 163 (1999) 93–102.
[42] D. Bhanushali, S. Kloos, C. Kurth, D. Bhattacharyya, J. Membr. Sci. 189 (2001) 1–21.
[43] S. Blumenschein, (2017).
[44] J. Robinson, J. Membr. Sci. 230 (2004) 29–37.
[45] D.o.R. Machado, D. Hasson, R. Semiat, J. Membr. Sci. 166 (2000) 63–69.
[46] H. Wang, M. Wang, X. Liang, J. Yuan, H. Yang, S. Wang, Y. Ren, H. Wu, F. Pan, Z. Jiang, Chem Soc Rev 50 (2021) 5468–5516.
[47] H. Moghadas, M.S. Saidi, N. Kashaninejad, N.T. Nguyen, Biomicrofluidics 12 (2018) 024117.
[48] A.R. Roudman, F.A. DiGiano, J. Membr. Sci. 175 (2000) 61–73.
[49] J.D. Hem, R. Minear, Water Analysis. Inorganic Species 1 (2012) 137–161.
[50] T.V.N. Nguyen, L. Paugam, P. Rabiller, M. Rabiller-Baudry, J. Membr. Sci. 601 (2020) 117907.
[51] J. Robinson, E. Tarletgton, A. Nijmeijer, Filtration-Coalville- 4 (2004) 50–56.
[52] E.J. Kappert, M.J.T. Raaijmakers, K. Tempelman, F.P. Cuperus, W. Ogieglo, N. E. Benes, J. Membr. Sci. 569 (2019) 177–199.